Check for updates

ADVANCED INTELLIGENT SYSTEMS
Open Access
www.advintellsyst.com

Versatile Standing Wave Generation Between Arbitrarily Oriented Surfaces Using Acoustic Metasurface Deflectors and Retroreflectors

*Chadi Ellouzi, Farhood Aghdasi, Ali Zabihi, Amir K. Miri, and Chen Shen**

Acoustic wave devices using standing wave configurations have gained interest in various fields like healthcare diagnostics and manufacturing. Their functionalities span from cell sorting to microscale fiber assembly through periodic acoustic pressure fields. Conventional methods usually require parallel acoustic emitters and reflective surfaces, producing constrained standing wave patterns. In this paper, an effective approach for creating versatile acoustic standing wave fields using an acoustic metasurface deflector and retroreflector is introduced. The deflector manipulates the direction of incoming acoustic waves coupled with the retroreflector to reflect these waves back to the source. The proposed design allows the creation of standing waves that are not constrained by the relative angles of the two surfaces involved and allows for customizable wave patterns beyond the standard limits with enhanced adaptability. The system's effectiveness is evaluated through computational simulations using finite element analysis and experimental validation based on a 3D-printed prototype. Results suggest that versatile standing waves between arbitrarily oriented surfaces can be produced through the careful design of the metasurface deflector and retroreflector. This approach can improve the performance of standing wave applications in particle manipulation, thus broadening the range of practical implementations for ultrasound and acoustofluidic technologies.

1. Introduction

Acoustic standing wave-based noncontact microparticle manipulation technique holds great promise in manufacturing, cell sorting, targeted drug release, and genetic disease diagnosis.[1–4] It features a straightforward setup, economical expense, substantial biocompatibility, and minimal contamination by reagents.[5–7] The associated acoustic radiation forces can be harnessed to handle microparticles with great precision and flexibility. Not surprisingly, numerous research efforts have harnessed the potential of standing waves for a wide range of utility across different media, with successful demonstrations reported in air, water, and other fluids.[8–10] Recently, this concept has been extended to ultrasound-based assembly and manufacturing, where forces induced by acoustic waves concentrate the particles. For example, a custom-made 3D printer nozzle, equipped with PZT transducers resonating at frequencies of 1, 1.5, and 2 MHz, was used to provide ultrasound self-assembly of microscale carbon fibers into a discontinuous line pattern within a photopolymer resin. The distribution of the microfibers was achieved by generating standing acoustic waves within the built-in PZT transducers in the nozzle, which aligned the fibers during the printing process.[11]

Additional research has embraced the use of standing waves within the field of acoustofluidics. Chen et al. engineered a device crafted from stainless steel for the nondestructive segregation of blood platelets. The approach used an integrated PZT transducer, resonating at a frequency of 225 kHz, affixed atop a microfluidic chamber to induce acoustic standing waves needed for the platelet separation.[12] Alternate studies have explored using acoustic waves to expedite the mixing process of microfluids. The approach involved generating acoustic multinode standing waves filed through the interaction of a PZT transducer, which can operate at frequencies up to 15 MHz, and the solid wall of the microfluidic channel, which serves as a reflecting surface.[13] Furthermore, other studies have employed a transducer resonating at 2 MHz to generate a free-flow acoustophoretic system. This approach enables the ongoing division of a heterogeneous mixture of polystyrene particles into several distinct outlet streams.[14] Other studies have employed a pair of transducers set in opposition to each other to create standing waves,[15,16] which necessitates precise adjustments in both transducers' frequency, phase, and amplitude. Such conditions demand intricate control measures and exceptional manufacturing precision.

C. Ellouzi, F. Aghdasi, A. Zabihi, C. Shen
Department of Mechanical Engineering
Rowan University
Glassboro, NJ 08028, USA
E-mail: shenc@rowan.edu

A. K. Miri
Department of Biomedical Engineering
New Jersey Institute of Technology
Newark, NJ 07102, USA

The ORCID identification number(s) for the author(s) of this article can be found under https://doi.org/10.1002/aisy.202400474.

© 2024 The Author(s). Advanced Intelligent Systems published by Wiley-VCH GmbH. This is an open access article under the terms of the Creative Commons Attribution License, which permits use, distribution and reproduction in any medium, provided the original work is properly cited.

DOI: 10.1002/aisy.202400474

26404567, 0, Downloaded from https://advanced.onlinelibrary.wiley.com/doi/10.1002/aisy.202400474, Wiley Online Library on [03/03/2025]. See the Terms and Conditions (https://onlinelibrary.wiley.com/terms-and-conditions) on Wiley Online Library for rules of use; OA articles are governed by the applicable Creative Commons License

Although considerable research has focused on contactless acoustic manipulation techniques, most studies require the use of two or more transducers or a reflector situated in a parallel configuration to generate the needed standing wave.[17,18] Furthermore, establishing standing waves with a tilted angle introduces difficulties that stem from the need for exact synchronization of the acoustic emitter and the reflecting surface and often require multiple differently oriented sources.[19] Maintaining a sharp inclination between the two components without compromising the integrity of the standing wave configuration can prove to be quite challenging. Studies indicate that within a channel with defined wall boundaries, these acoustic waves can be harnessed to generate stable diffractive patterns maintained over time, thanks to the constraints provided by the transducer area.[20–23] One significant constraint of such diffraction-based techniques is that the acoustic waves are unavoidably aligned parallel to the channel boundaries, making the geometry of the fluidic environment inherently intertwined with the acoustic one. This intrinsic coupling restricts the practicality of these methods for applications that require continuous processing and the creation of complex acoustic wave patterns.

In this work, we created acoustic standing wave fields at various angles using acoustic metasurface deflectors and retroreflectors. Acoustic metasurfaces have significantly broadened the manipulation of acoustic fields through various functionalities[24,25] including wavefront modulation,[26–28] frequency-selective transmission,[29–31] energy absorption,[32,33] and so on. Here, the acoustic metasurface deflector design is based on the generalized Snell's law. In contrast, the retroreflector's design adheres to the principles of the grating equation. The configuration of both surfaces is meticulously crafted to ensure that they can modulate acoustic waves during both the incidence and reflection stages. This approach enables the customization of standing wave patterns between any two surfaces, regardless of their orientation, and permits the manipulation of standing wave fields at multiple predetermined angles. The performance of this integrated system was assessed through computational modeling and experimental tests involving hydrophone needle measurements. The results reveal that with careful engineering of the metasurface deflector and retroreflector, it is possible to sustain standing waves at various angles relative to their surfaces. This system presents a convenient approach for generating standing waves at diverse frequencies and orientations that are unachievable with conventional methods.

2. Numerical Analysis

2.1. Design of the Metasurface Deflector and Retroreflector for Standing Wave Generation

Developing a system that combines the ability to modulate incoming and reflected waves is required to relax the constraint of aligning the acoustic source with the reflector to produce standing waves. **Figure 1** illustrates the overall proposed system configuration needed for standing wave generation. The metasurface deflector bends the incoming plane wave towards a specific angle, whereas the retroreflector reflects the wave back in its original direction, facilitating the formation of a standing wave. Since the metasurface deflector and retroreflector can be designed to accommodate various wave angles, the generation of standing waves does not depend on the orientation of the involved surfaces, thus enhancing the flexibility of the proposed system. Consider an ultrasound wave incident from the x-direction at an incident angle θ_i, the metasurface deflector is designed based on the generalized Snell's law as follows[34]

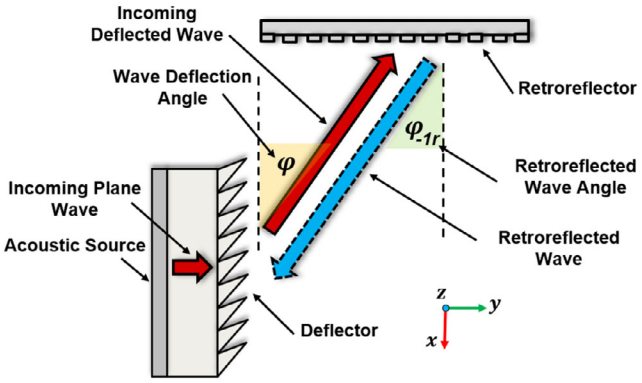

Figure 1. Schematic of the proposed standing wave generation system. A standing wave can be generated between both surfaces by bending the incident wave using the deflector and reflecting it back with the retroreflector. The standing wave angle can be adjusted by modulating the deflected and reflected waves and does not depend on the angle between both surfaces.

$$k_x^r = k_x + mG + \frac{\partial \varphi}{\partial x} \tag{1}$$

In the given context, $k_x = k\sin(\theta_i)$ and $k_x^r = k\sin(\theta_r)$ are the wave vectors of the incident and transmitted waves, respectively, with θ_r denoting the refraction angle. The term $k = \frac{2\pi}{\lambda}$ represents the wave vector in the refraction medium and λ is its corresponding wavelength while $\frac{\partial \varphi}{\partial x}$ is the surface phase gradient. $G = \frac{2\pi}{\Gamma}$ is the amplitude of the reciprocal lattice vector and m is the diffraction order caused by the periodicity Γ of the deflector. However, the direct implementation of Equation (1) leads to suboptimal performance of the metasurface deflector, as shown in **Figure 2**a, exemplifying a 45° wavefront modulation. This is due to acoustic wave leakage across the various deflector subunits, coupled with internal interference among them. This can be attributed to the lack of an acoustic rigid boundary to clearly separate each subunit of the deflector. Unlike airborne acoustic waves in which sound hard boundaries can be easily fulfilled by solid materials,[35,36] underwater ultrasound's acoustic impedance contrast is much smaller. The waves naturally diffract within the metasurface deflector. Thus, a uniform phase gradient cannot be maintained at the output surface of the metasurface deflector, deteriorating its performance and generating undesired diffraction modes.

An optimization process was implemented to enhance the metasurface deflector's performance. The aim was to enhance the refraction efficiency of the metasurface deflector by

© 2024 The Author(s). Advanced Intelligent Systems published by Wiley-VCH GmbH

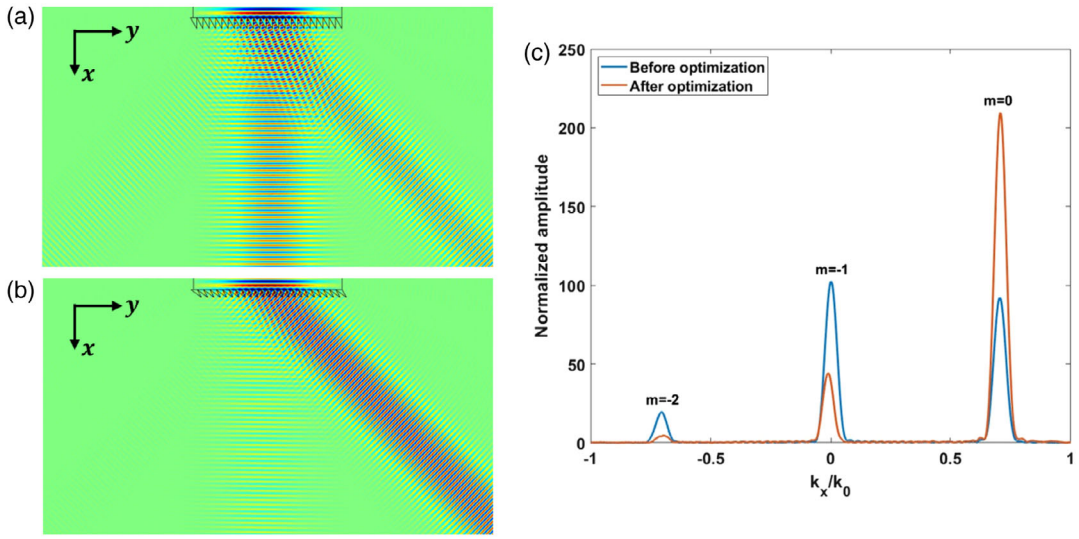

Figure 2. The designed deflector performance optimization for a 45° case. The performance of the metasurface deflector a) before and b) after optimization. c) Normalized wave pressure of different diffraction orders for the metasurface deflector before and after optimization. Undesired diffraction modes ($m = -1$ and $m = -2$) are significantly suppressed by optimizing the structure.

suppressing the undesired refraction modes. The structural configuration was adjusted by including an angular tilt to the edge of each unit[37] in addition to an optimized extrusion thickness to ensure optimal deflector performance. The optimization analysis concluded that a tilt angle $\alpha_G = 74°$ with a periodic length $p = 2.12$ mm results in optimal performance for the 45° wave deflection case. This finding is clearly illustrated in Figure 2b. Figure 2c depicts the calculated normalized amplitude of each diffraction order, confirming that the desired mode ($m = 0$) is maximized, while others are suppressed. To facilitate ease in 3D printing, the metasurface deflector's base height was included, resulting in an overall thickness of $h_{max} = 10.2$ mm of the deflector. For the case of the retroreflector surface, the period $p = 2.12$ mm, width $w = 0.487$ mm, and depth $h = 0.321$ mm of groove per unit cell were determined for a total reflection at 45° based on a multiobject optimization generic algorithm.[38] Visual depictions of the metasurface retroreflector and deflector can be seen in **Figure 3**.

2.2. Numerical Simulation

The system's effectiveness in generating and sustaining pressure standing wave field was first demonstrated using finite element simulations in COMSOL Multiphysics software. All the media were considered to be linear and isotropic in the simulation. A frequency domain-based model that couples pressure acoustics with solid mechanics was employed. The deflector and the retroreflector were modeled as elastic materials. The metasurface deflector, retroreflector, and background medium material were defined as cured SLA resin, steel, and water, respectively. The following material properties were used for the deflector and retroflector respectively: $\rho_l = 1178\ \mathrm{kg\,m^{-3}}$, $c_l = 1860\ \mathrm{m\,s^{-1}}$, $\nu_l = 0.33$, $E_l = 2.75$ GPa, and $\rho_s = 7850\ \mathrm{kg\,m^{-3}}$, $c_s = 5940\ \mathrm{m\,s^{-1}}$, $\nu_s = 0.27$, $E_s = 210$ GPa respectively.[39] For the water, the values are $\rho_m = 1000\ \mathrm{kgm^{-3}}$ and $c_m = 1490\ \mathrm{m\ s^{-1}}$. A Gaussian beam with an acoustic excitation frequency of 1 MHz was established at the source location to generate incident waves. In all the

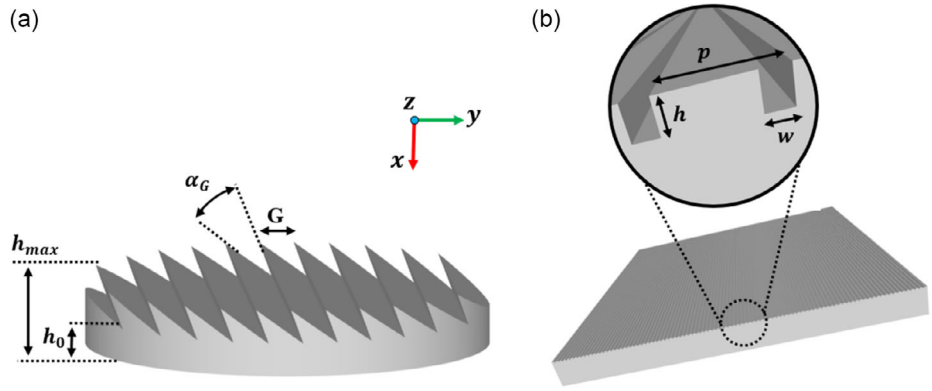

Figure 3. The designed metasurface geometry. a) Metasurface deflector. b) Metasurface retroreflector. The inset illustrates the geometric parameters used in the design.

© 2024 The Author(s). Advanced Intelligent Systems published by Wiley-VCH GmbH

26404567, 0, Downloaded from https://advanced.onlinelibrary.wiley.com/doi/10.1002/aisy.202400474, Wiley Online Library on [03/03/2025]. See the Terms and Conditions (https://onlinelibrary.wiley.com/terms-and-conditions) on Wiley Online Library for rules of use; OA articles are governed by the applicable Creative Commons License

simulations, perfectly matched layers surrounding all the edges of the simulation domain were applied to minimize reflections at the boundaries. A series of two main scenarios were subjected to numerical simulation. In the first set of scenarios, the metasurface deflector and the retroreflector surfaces were arranged in a parallel manner with respect to each other but with a generated standing wave field at angles of $\theta = 30°, \theta = 45°$, and $\theta = 60°$ relative to the x-axis, respectively. For the second set of scenarios, a standing wave field is generated between the deflector and the retroreflector surfaces, which are arranged in $\beta = 60°$, $\beta = 90°$ and $\beta = 120°$ angle between each other relative to the y-axis, respectively.

The simulation results for the first set of scenarios and angles demonstrated that the behavior of the acoustic wave, specifically its refraction and reflection within the system, aligned with the expected results as illustrated in **Figure 4**. These expectations were based on theoretical understanding and corroborated by established research about acoustic metasurfaces used as deflectors and retroreflectors.[40] Different standing wave patterns were generated by controlling the incident and reflected waves, showcasing the system's flexibility in configuring the wave profile. This can be challenging to obtain using conventional approaches, where the standing waves are always parallel to the surfaces.

Notably, in the second set of scenarios and using the same concept, nonparallel deflector–retroreflector system configuration demonstrated the ability to generate a stable standing waves pattern even when both metasurfaces are positioned with a wide angle with respect to each other, which is challenging to achieve with conventional approaches, as can be seen in **Figure 5**. In both scenarios, undesired diffraction modes or reflections were minimized thanks to the high efficiency of the metasurfaces. Computational analyses suggest that the total energy efficiency

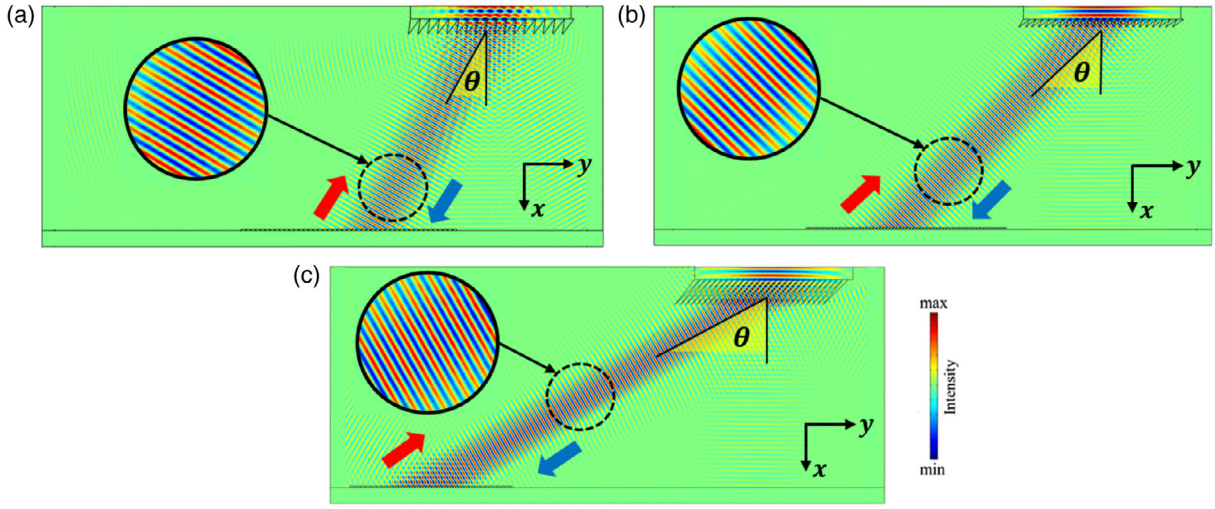

Figure 4. The simulated standing wave generated in parallel deflector–retroreflector system configuration. a) Deflector–retroreflector deflected wave angle $\theta = 30°$. b) Deflector–retroreflector deflected wave angle $\theta = 45°$. c) Deflector–retroreflector deflected wave angle $\theta = 60°$.

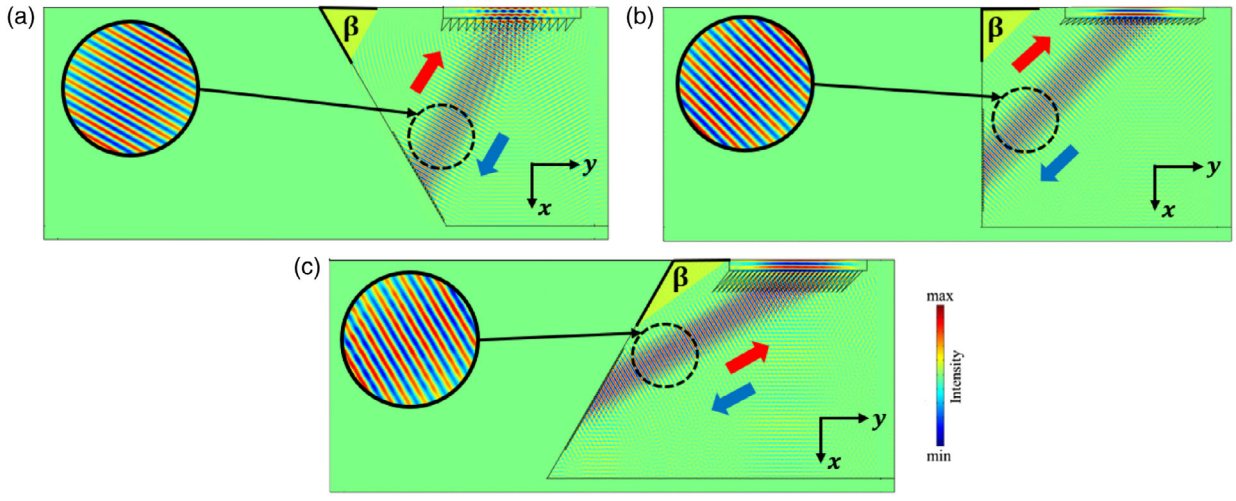

Figure 5. The simulated standing wave generated between nonparallel surfaces with different angles. a) Deflector–retroreflector angle $\beta = 60°$. b) Deflector–retroreflector angle $\beta = 90°$. c) Deflector–retroreflector angle $\beta = 120°$.

© 2024 The Author(s). Advanced Intelligent Systems published by Wiley-VCH GmbH

26404567, 0, Downloaded from https://advanced.onlinelibrary.wiley.com/doi/10.1002/aisy.202400474, Wiley Online Library on [03/03/2025]. See the Terms and Conditions (https://onlinelibrary.wiley.com/terms-and-conditions) on Wiley Online Library for rules of use; OA articles are governed by the applicable Creative Commons License

of the proposed system (η_{system}) is 90.66%, highlighting the system's effectiveness and stability. The bandwidth of the system reaching 80% efficiency is around 0.05 MHz, which is relatively small due to the fact that both metasurfaces are designed at a single frequency. Nevertheless, the bandwidth can always be improved by adopting optimization techniques such as topology optimization and genetic algorithm if needed.[41,42]

3. Experimental Results

To assess the performance of the proposed setup, a functional prototype was constructed. As an example, a metasurface deflector and a corresponding retroreflector configured at a 90° angle to each other were chosen to produce an illustrative 45° tilted standing wave as a proof of concept. The metasurface deflector and retroreflector were made using a Formlab stereolithography 3D printer and micromachining CNC machine, respectively, which offer superior print and machining resolution. The SLA resin was used in printing the deflectors due to its sound speed property which contrasts with that of water, allowing for modulation of the transmitted phase. On the other hand, the acoustic impedance of this resin is sufficiently close to that of water, which promotes a comparatively high transmission coefficient. For the retroreflector, stainless steel was selected to optimize the reflectivity of the surface. This choice ensures a rigid boundary condition, reducing the absorption of sound while keeping the production process both simple and cost-effective. The metasurface deflector had a diameter of 49 mm, with a base height of 4 mm, and a peak height of 10.2 mm at the deflector unit extremities. The retroreflector metasurface measured 100 mm in both length and width, respectively. **Figure 6** illustrates the completed 3D-printed metasurface deflector and the machined retroreflector surface used for the experiments.

After the printing, the metasurface deflector was mounted on a ceramic circular piezoelectric transducer (SMR, Davenport, FL) that matched the deflector at 49 mm in diameter and had a thickness of 2 mm, with a 1 MHz resonance frequency to provide the necessary acoustic actuation. A function generator (RIGOL DG4162, Portland, OR) was used to generate a plane wave. The output signal was then amplified through an RF power amplifier (ENI 3200L, Renton, WA) to ensure a sufficient incident acoustic wave intensity. During the experiment, the

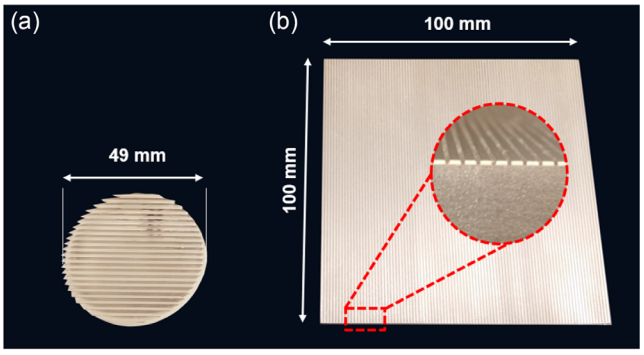

Figure 6. a) The 3D printed acoustic deflector and the b) micro-machined retroreflector surface used for the 45° standing wave generation case.

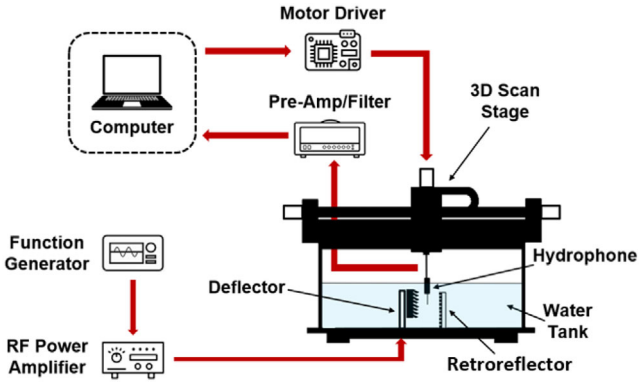

Figure 7. The schematic of the measurement setup used for the standing wave data collection.

standing wave pattern was assessed with the help of a hydrophone (Precision Acoustics NH0500, Dorchester, UK) positioned on a 3D scanning stage. **Figure 7** delineates the layout of the experimental setup used for this purpose. Initial data from the experiment were captured by the hydrophone via a 5 mm acoustic needle and subsequently analyzed with specialized software. To maintain the waveform data's accuracy and eliminate unwanted background noise, a Butterworth filter with a cutoff frequency of 10 Hz was applied. Furthermore, a sliding window approach was adopted to retain the main signal and truncated data outside the primary event, thus eliminating any extraneous reflected waves.

Throughout the experiment, an extensive grid scan was undertaken, involving 80 steps with 0.5 mm each along both the x and y axes, with 125 000 individual data points captured and extracted from the oscilloscope's memory at different points along the scanning path of the hydrophone. The established scanning grid covered a region between the metasurface deflector and the retroreflector, measured 40 mm by 40 mm, which allowed for a more detailed analysis and graphical depiction of the pressure amplitude information produced by the system. The data gathered from the experiment, specifically about the system's performance with a 45° titled standing wave setup, are depicted in **Figure 8**.

The experimental results from the specific scenario of a pressure field tilted at 45 degrees, produced by the deflector–retroreflector arrangement, strongly correlate with the computational predictions and analytical calculations. The metasurface deflector adeptly redirected the wave emitted by the transducer towards the intended angle due to the deflector's capacity to introduce a phase shift across its surface. This phase modulation technique enables accurate redirecting of the acoustic beam in any chosen direction, owing to the carefully designed grating cells that, in this instance, were tailored for redirecting the wave at a 45° angle. Similarly, the retroreflector metasurface showed high efficiency in retroreflecting nearly all the incoming acoustic waves that the acoustic deflector redirected, forming a completely integrated system that could produce the pressure field depicted in Figure 2b. The experimentally created standing wave exhibited a tilt of 44.7°, aligning closely with the anticipated 45° angle predicted by simulations. This experimental result for the standing

© 2024 The Author(s). Advanced Intelligent Systems published by Wiley-VCH GmbH

26404567, 0, Downloaded from https://advanced.onlinelibrary.wiley.com/doi/10.1002/aisy.202400474, Wiley Online Library on [03/03/2025]. See the Terms and Conditions (https://onlinelibrary.wiley.com/terms-and-conditions) on Wiley Online Library for rules of use; OA articles are governed by the applicable Creative Commons License

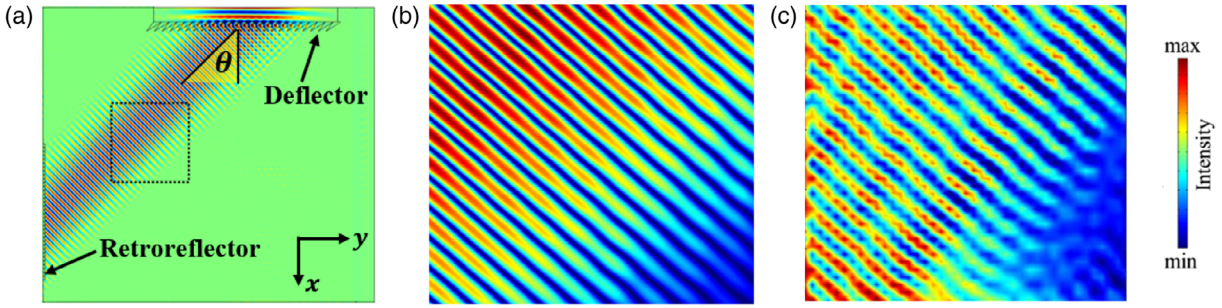

Figure 8. The 45° tilted pressure field generated in the deflector–retroreflector system. a) The overall experimental configuration through simulation. b) Zoom-in view of the numerical results of the dotted box in (a). c) Experimental result of the dotted box area in (a).

wave tilted at 45° validates the concept that with careful design and the combination of various acoustic deflectors, it is feasible to generate tilted pressure fields at a broad range of angles. This can be done without an intricate transducer arrangement or complex structural adjustments to ensure parallel surfaces in the first place. Other designs showcased in Figure 4 are expected to exhibit the same level of performance. This method offers considerable flexibility for various projects investigating acoustic standing wave formations, owing to its adaptable nature combined with a simple design and manufacturing procedure.

Despite the expectations, there were some mismatches between the theoretical models and the actual experimental results. The standing wave patterns generated in practice did not match the sharpness and clarity predicted by the simulations. The observed discrepancies between the simulated results and experimental data could stem from a range of factors. For example, manufacturing imperfections could cause slight deviations in the shape of the deflector's profile and irregularities on the retroreflector's surface. Furthermore, the metasurface deflector surface may exhibit unevenness due to residual layers of hardened resin in the spaces between grating cells, leading to unwanted refractive effects. The slight variations in the sound speed values used in the design and the experiment, and the inevitable losses in the lab environment could be possible reasons for the differences in the result. Nevertheless, enhancing the transducer's performance, refining the fabrication of the acoustic deflector unit cells, optimizing the 3D scanning system, and decreasing the step size in data collection, can mitigate the previously mentioned experimental inaccuracies.

4. Conclusion

This research proposes an integrated acoustic system based on metasurfaces capable of generating acoustic standing wave patterns at various tilted angles theoretically and experimentally. The design features a metasurface deflector, which takes acoustic waves from a piezoelectric transducer and steers them toward predetermined directions. Furthermore, a retroreflector is incorporated into the system, ensuring complete reflection of these steered waves at specially engineered angles, thus creating a specific pattern of pressure fields. This approach offers greater flexibility and adaptability by eliminating the need for complex transducer configurations and elaborate experimental arrangements that were once essential to produce such angled pressure distributions, particularly at extreme angles. Theoretical calculations related to the design of the system components were carried out using custom-made scripts. At the same time, acoustics-frequency domain simulations were made for the different proposed scenarios using COMSOL Multiphysics. The simulations confirmed that the performance of the proposed acoustic system aligned with the predictions based on theoretical understanding and the body of knowledge surrounding metasurfaces used for acoustic wave manipulation. Using a PZT transducer with a resonance frequency of 1 MHz, the outcomes substantiated the creation of a pressure standing wave field. This was made apparent due to the clear presence of zones of intensified pressure alongside identifiable pressure nodal points. The findings were further supported by an experimental validation approach by creating a 45° angled standing wave as an example using the proposed acoustic deflector–retroreflector system. It is important to recognize that while the suggested metasurfaces system is capable of operating with high efficiency at moderate angles, there is a limitation when dealing with large angles. Specifically, employing only a phase shift approach in such a scenario will result in reduced efficiency because of impedance mismatch. However, this constraint can potentially be mitigated by incorporating bianistropic building blocks[43,44] or impedance-based designs[45,46] into the proposed metasurfaces. Our research expands the possibilities beyond the conventional scope of standing wave generations, which, through intensive optimization of the proposed system, can be expanded even further to operate in a broader frequency range, thereby elevating their importance in fields such as biomedicine and regulation of biological entities within living organisms.[47–49]

This research casts a fresh perspective on 3D phenomena, opening the door to intriguing future investigations concerning using acoustic standing waves in 3D environments via the application of metasurfaces. The proposed approach provides benefits in a variety of applications, such as advanced additive manufacturing.[50,51] For example, using a single, pre-engineered metasurface deflector could streamline the creation of standing waves at acute angles that are hard to generate, significantly reducing the reliance on complex tweezer systems and improving the overall effectiveness and straightforwardness of the experimental configuration. In addition, the metasurfaces may be combined with tunable designs[52] to realize reconfigurable

© 2024 The Author(s). Advanced Intelligent Systems published by Wiley-VCH GmbH

26404567, 0, Downloaded from https://advanced.onlinelibrary.wiley.com/doi/10.1002/aisy.202400474, Wiley Online Library on [03/03/2025]. See the Terms and Conditions (https://onlinelibrary.wiley.com/terms-and-conditions) on Wiley Online Library for rules of use; OA articles are governed by the applicable Creative Commons License

and adaptive standing wave generation. Our proposed approach could pave the way for innovative techniques not only in advanced additive manufacturing technologies but also in the segregation of biological specimens by their type, as well as the future enhancement of medical instruments.

Acknowledgements

This work was supported by the National Science Foundation (CBET-2243507 and ECCS-2337069) and the New Jersey Health Foundation (PC 85-23).

Conflict of Interest

The authors declare no conflict of interest.

Author Contributions

Chadi Ellouzi: Data curation (equal); Formal analysis (equal); Methodology (equal); Writing—original draft (equal); Writing—review and editing (equal). **Farhood Aghdasi**: Formal analysis (equal); Methodology (equal); Writing—review and editing (equal). **Ali Zabihi**: Formal analysis (equal); Methodology (equal); Writing—review and editing (equal). **Amir K. Miri**: Methodology (equal); Supervision (equal); Writing—review and editing (equal). **Chen Shen**: Conceptualization (equal); Formal analysis (equal); Funding acquisition (equal); Supervision (equal); Writing—review and editing (equal).

Data Availability Statement

The data that support the findings of this study are available from the corresponding author upon reasonable request.

Keywords

acoustic metasurface, acoustic waves, acoustofluidics, standing wave, ultrasound

Received: June 11, 2024
Revised: August 7, 2024
Published online:

[1] Y. Sriphutkiat, Y. Zhou, *Sens. Actuators A Phys.* **2017**, *263*, 521.
[2] W. Liu, H. Gao, K. Liu, D. Lei, K. Pei, G. Hu, *J. Nanopart. Res.* **2022**, *24*, 81.
[3] A. G. Guex, N. Di Marzio, D. Eglin, M. Alini, T. Serra, *Mater Today Bio* **2021**, *10*, 100110.
[4] K. Yiannacou, V. Sariola, *Adv. Intell. Syst.* **2023**, *5*, 2300058.
[5] S. P. Zhang, J. Lata, C. Chen, J. Mai, F. Guo, Z. Tian, L. Ren, Z. Mao, P.-H. Huang, P. Li, S. Yang, T. J. Huang, *Nat. Commun.* **2018**, *9*, 2928.
[6] J. Friend, L. Y. Yeo, *Rev. Mod. Phys.* **2011**, *83*, 647.
[7] X. Ding, P. Li, S.-C. S. Lin, Z. S. Stratton, N. Nama, F. Guo, D. Slotcavage, X. Mao, J. Shi, F. Costanzo, T. J. Huang, *Lab Chip* **2013**, *13*, 3626.
[8] C. M. G. Atehortúa, N. Pérez, M. A. B. Andrade, L. O. V. Pereira, J. C. Adamowski, *Ultrason. Sonochem.* **2019**, *57*, 57.
[9] M. A. B. Andrade, N. Pérez, J. C. Adamowski, *Appl. Phys. Lett.* **2015**, *106*, 14101.
[10] A. Marzo, S. A. Seah, B. W. Drinkwater, D. R. Sahoo, B. Long, S. Subramanian, *Nat. Commun.* **2015**, *6*, 8661.
[11] P. Wadsworth, I. Nelson, D. L. Porter, B. Raeymaekers, S. E. Naleway, *Mater. Des.* **2020**, *185*, 108243.
[12] Y. Chen, M. Wu, L. Ren, J. Liu, P. H. Whitley, L. Wang, T. J. Huang, *Lab Chip* **2016**, *16*, 3466.
[13] C. Pothuri, M. Azharudeen, K. Subramani, *Phys. Fluids* **2019**, *31*, 122001.
[14] F. Petersson, L. Åberg, A.-M. Swärd-Nilsson, T. Laurell, *Anal. Chem.* **2007**, *79*, 5117.
[15] A. Ozcelik, *Actuators* **2022**, *11*, 249.
[16] A. Struckas, P. Vasiljev, R. Bareikis, S. Borodinas, J. Kasperoviciene, *Sens. Actuators A Phys.* **2017**, *263*, 754.
[17] H. Bruus, *Lab Chip* **2012**, *12*, 20.
[18] A. Lenshof, M. Evander, T. Laurell, J. Nilsson, *Lab Chip* **2012**, *12*, 684.
[19] Z. Tian, S. Yang, P.-H. Huang, Z. Wang, P. Zhang, Y. Gu, H. Bachman, C. Chen, M. Wu, Y. Xie, T. J. Huang, *Sci. Adv.* **2019**, *5*, eaau6062.
[20] C. Devendran, K. Choi, J. Han, Y. Ai, A. Neild, D. J. Collins, *Lab Chip* **2020**, *20*, 2674.
[21] D. J. Collins, R. O'Rorke, A. Neild, J. Han, Y. Ai, *Soft Matter* **2019**, *15*, 8691.
[22] A. Fakhfouri, C. Devendran, T. Albrecht, D. J. Collins, A. Winkler, H. Schmidt, A. Neild, *Lab Chip* **2018**, *18*, 2214.
[23] D. J. Collins, R. O'Rorke, C. Devendran, Z. Ma, J. Han, A. Neild, Y. Ai, *Phys. Rev. Lett.* **2018**, *120*, 074502.
[24] Z. Zhang, W. Xiang Jiang, X. Ge Zhang, W. Kang Cao, L. Bai, C.-W. Qiu, T. Jun Cui, *Mater. Des.* **2023**, *229*, 111903.
[25] A. Zabihi, C. Ellouzi, C. Shen, *Front. Mater.* **2023**, *10*, 1132585.
[26] Y. Xie, W. Wang, H. Chen, A. Konneker, B.-I. Popa, S. A. Cummer, *Nat. Commun.* **2014**, *5*, 5553.
[27] H. Zhao, C. Zhang, J. He, Y. Li, B. Li, X. Jiang, D. Ta, *Front. Mater.* **2022**, *8*, 802001.
[28] S. Zhao, N. Zhang, P. Han, Y. Gu, H. Dong, *Small* **2024**, *20*, 2308349.
[29] X. Jiang, Y. Li, B. Liang, J. Cheng, L. Zhang, *Phys. Rev. Lett.* **2016**, *117*, 034301.
[30] C. Ellouzi, A. Zabihi, F. Aghdasi, A. Kayes, M. Rivera, J. Zhong, A. Miri, C. Shen, *APL Mater.* **2024**, *12*, 031130.
[31] C. Ellouzi, A. Zabihi, L. Gormley, F. Aghdasi, K. Stojanoska, A. Miri, R. Jha, C. Shen, *J. Acoust. Soc. Am.* **2024**, *155*, 1759.
[32] G. N. Almeida, E. F. Vergara, L. R. Barbosa, A. Lenzi, P. H. Mareze, R. S. Birch, *Phys. Lett. A* **2022**, *451*, 128417.
[33] H. Baali, M. Addouche, A. Bouzerdoum, A. Khelif, *Commun. Mater.* **2023**, *4*, 40.
[34] G. Liao, C. Luan, Z. Wang, J. Liu, X. Yao, J. Fu, *Adv. Mater. Technol.* **2021**, *6*, 2000787.
[35] X.-F. Zhu, S.-K. Lau, *J. Appl. Phys.* **2019**, *126*.
[36] J. Lan, X. Zhang, X. Liu, Y. Li, *Sci. Rep.* **2018**, *8*, 14171.
[37] Y. Liu, G. Qu, X. Jiang, J. Han, Z. Ji, Z. Liu, Q. Song, S. Yu, S. Xiao, *Laser Photon. Rev.* **2023**, *17*, 2200712.
[38] L.-S. Zeng, Y.-X. Shen, X.-S. Fang, Y. Li, X.-F. Zhu, *Ultrasonics* **2021**, *117*, 106548.
[39] M. Bakaric, P. Miloro, A. Javaherian, B. T. Cox, B. E. Treeby, M. D. Brown, *J. Acoust. Soc. Am.* **2021**, *150*, 2798.
[40] B. Liu, B. Ren, J. Zhao, X. Xu, Y. Feng, W. Zhao, Y. Jiang, *Appl. Phys. Lett.* **2017**, *111*, 252602.
[41] H.-W. Dong, C. Shen, S.-D. Zhao, W. Qiu, H. Zheng, C. Zhang, S. A. Cummer, Y.-S. Wang, D. Fang, L. Cheng, *Nat. Sci. Rev.* **2022**, *9*, nwac030.
[42] Z. Li, Y. Sun, G. Wu, M. Tao, *Appl. Acoust.* **2023**, *204*, 109247.
[43] A. Díaz-Rubio, J. Li, C. Shen, S. A. Cummer, S. A. Tretyakov, *Sci. Adv.* **2019**, *5*, eaau7288.

© 2024 The Author(s). Advanced Intelligent Systems published by Wiley-VCH GmbH

26404567, 0, Downloaded from https://advanced.onlinelibrary.wiley.com/doi/10.1002/aisy.202400474, Wiley Online Library on [03/03/2025]. See the Terms and Conditions (https://onlinelibrary.wiley.com/terms-and-conditions) on Wiley Online Library for rules of use; OA articles are governed by the applicable Creative Commons License

[44] Y.-Z. Tian, Y.-F. Wang, V. Laude, Y.-S. Wang, *Commun. Phys.* **2024**, *7*, 34.
[45] J. Li, C. Shen, A. Díaz-Rubio, S. A. Tretyakov, S. A. Cummer, *Nat. Commun.* **2018**, *9*, 1342.
[46] Y. K. Chiang, S. Oberst, A. Melnikov, L. Quan, S. Marburg, A. Alù, D. A. Powell, *Phys. Rev. Appl.* **2020**, *13*, 064067.
[47] X. Peng, W. He, F. Xin, G. M. Genin, T. J. Lu, *J. Mech. Phys. Solids* **2020**, *145*, 104134.
[48] F. Guo, Z. Mao, Y. Chen, Z. Xie, J. P. Lata, P. Li, L. Ren, J. Liu, J. Yang, M. Dao, S. Suresh, T. J. Huang, *Proc. Natl. Acad. Sci. U.S.A.* **2016**, *113*, 1522.
[49] O. Pourmehran, K. Zarei, J. Pourchez, S. Vreugde, A. Psaltis, P.-J. Wormald, *Int. J. Pharm.* **2023**, *644*, 123277.
[50] M. D. Haslam, B. Raeymaekers, *Compos. B Eng.* **2014**, *60*, 91.
[51] J. Greenhall, B. Raeymaekers, *Adv. Mater. Technol.* **2017**, *2*, 1700122.
[52] K. Zeng, Z. Li, Z. Guo, Z. Wang, *Adv. Phys. Res.* **2024**, *3*, 2300128.

© 2024 The Author(s). Advanced Intelligent Systems published by Wiley-VCH GmbH

26404567, 0, Downloaded from https://advanced.onlinelibrary.wiley.com/doi/10.1002/aisy.202400474, Wiley Online Library on [03/03/2025]. See the Terms and Conditions (https://onlinelibrary.wiley.com/terms-and-conditions) on Wiley Online Library for rules of use; OA articles are governed by the applicable Creative Commons License